Chaotic motion of nonspherical particles settling in a cellular flow field

H. Shin
R & D Center, Samsung Electronics Company, Suwon City, Kyungki-Do, Korea 441-742

M. R. Maxey
Division of Applied Mathematics, Brown University, Providence, Rhode Island 02912
(Received 14 February 1997)

Small, spheroidal particles undergo a tumbling motion as they settle out under gravity through a fluid flow. This motion is in response to the fluid forces that act on the particle causing it to rotate due to the local fluid vorticity and rate of strain. In this paper the nonlinear system of differential equations governing the particle motion in a spatially periodic, cellular flow field is considered. The motion of spherical particles is completely regular, and in some regions of the flow they may be permanently suspended. Using recent results on volume-preserving maps, it is shown that this behavior can persist for nonspherical particles. More usually the tumbling motion is chaotic. This is characterized by results on Poincaré sections of the motion and determination of Lyapunov exponents. The response to flow vorticity and rate of strain is analyzed for both full three-dimensional motion and restricted planar motion to determine the main factors governing the chaotic motion. [S1063-651X(97)01111-2]

PACS number(s): 47.52.+j, 47.55.kf, 05.45.+b

I. INTRODUCTION

A recurring question in the study of particle settling is whether or not particles can be held in suspension by a flow. The gravitational settling of small, spherical particles in a steady convection flow was studied by Stommel [1]. He showed that if the convective updraft was greater than the terminal fall speed of the particle then in a region of the flow particles will be permanently held in suspension, as illustrated in Fig. 1. Later work by Maxey and Corrsin [2] and Maxey [3] revealed that if the inertial effects of the particles are included the permanent suspension is no longer maintained and all the particles eventually settle out. Unlike the above studies, Smith and Spiegel [4] observed a chaotic motion by introducing spherical particles into an unsteady cellular flow field. Crisanti *et al.* [5] quantitatively studied the motion of spherical particles in a steady two-dimensional cellular flow where the particles exhibited strong inertia in their response to local fluid velocity. Here too they found that the particle motion was chaotic for particles slightly heavier than the fluid. This kind of chaotic motion, of either discrete particles or of fluid elements, known as Lagrangian turbulence [6] has also been analyzed in the steady incompressible three dimensional *ABC* flow of Arnold [7] by Dombre *et al.* [8]. They observed that the Lagrangian motion of fluid elements in ABC flow is chaotic in the neighborhood of the heteroclinic lines connecting the unstable fixed points. More recent studies [9,10] on the motion of solid particles in the *ABC* flow have shown that both small- and large-particle inertia, as compared to a characteristic flow time scale, eliminated chaos but for intermediate particle inertia the Lagrangian motion was chaotic.

Frequently the particles encountered in engineering or natural contexts such as the formation and growth of crystals in a liquid melt, ice crystal growth in atmospheric clouds [11], or the formation of crystals in a cooling body of magma [12] are nonspherical. Yet despite their prevalence there is much less information available on the characteristics of their motion. Spheroidal particles and ellipsoids of revolution are the simplest examples of nonspherical particles to consider, and their orientation can be characterized by a simple unit vector **m** along the axis of symmetry. An early study of the motion of nonspherical particles in a fluid was the paper by Jeffrey [13]. He considered an ellipsoidal particle which was neutrally buoyant and was placed in a uniform shear flow. The forces and moments acting on the small particle were determined from the low Reynolds number Stokes flow produced locally by the particle moving relative to the flow. In this example the center of the particle moved with the local fluid velocity but the particle turned continuously in response to the vorticity and the rate of strain of the uniform shear flow. Extensions to these results are given by Bretherton [14] and Happel and Brenner [15] for particles within the Stokes regime. Extending the results of Jeffrey [13] for single particles, Davis [16] has considered the average sedimentation velocity in a dilute suspension of axisymmetric particles suspended in a simple shear flow at low-particle Reynolds numbers. He noted the dependence of the sedimentation of the particles on their shapes and orientations and the rotation of the particles by the imposed flow field.

The motion of rigid spheroidal particles settling under gravity in a cellular flow field was first investigated by Mallier and Maxey [17]. Along with both settling motion of some particles and a permanent suspension of others, they detected the onset of chaotic motion at large particle aspect ratios. In a separate context a suspension of neutrally buoyant, nonsettling, spheroidal particles has been used as an example of a fluid with complex microstructure. Szeri, Wiggins, and Leal [18] studied this for the dynamical behavior of an orientable microstructure in a general two-dimensional fluid flow. They emphasized the fact that the usual tools for analysis of an autonomous system should not be casually applied to the analysis of a nonautonomous system. They

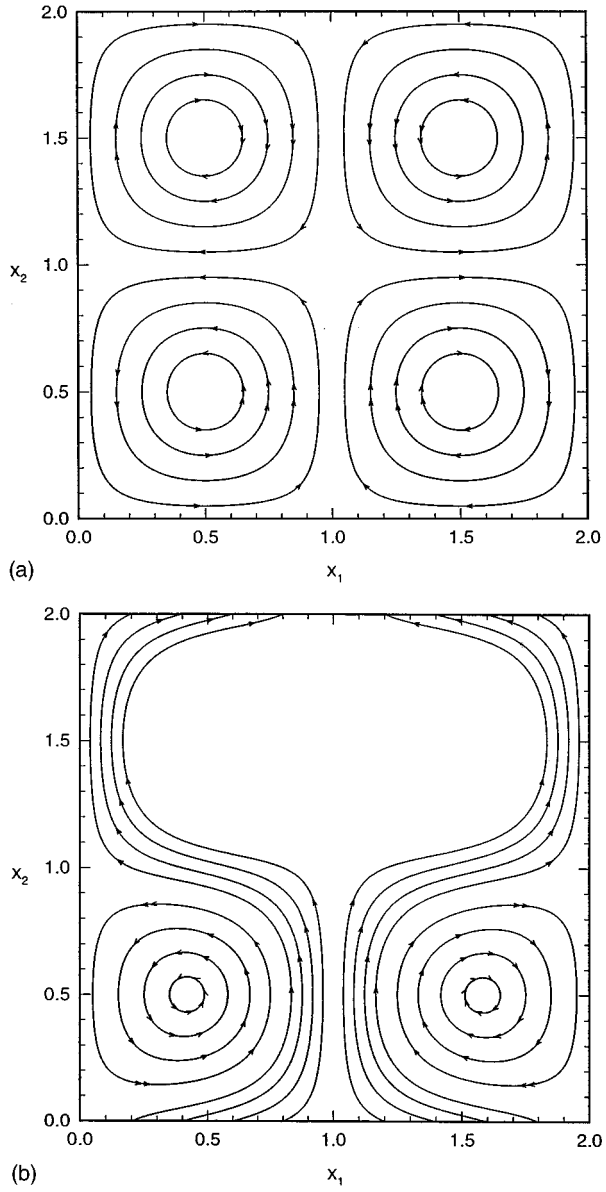

FIG. 1. Particle trajectories in vertically aligned cellular flow: (a) Lagrangian fluid particles; (b) spherical particles with terminal fall speed $W_1 = 0.025$. Note that ''settling'' is in the direction of x_2 increasing, the arrows indicate the direction of motion. For (b), initial particle positions are along $x_2 = 0$ or 0.5 only.

developed instead a contraction exponent to describe the attraction or repulsion of a particular orbit from neighboring orbits and applied this to consider the out-of-plane and stretching motion of the microstructure. Szeri and Leal [19] later developed a computational method to solve flow problems of microstructured fluids considering the distribution function of the conformation of the local structure, for which explicit knowledge is not required and which involves no approximation.

In extending the work of Mallier and Maxey [17], the purpose of this study is to determine more precisely the nature of the chaotic motion mentioned in their work, whether it is observed for all initial particle positions and orientations and what effect the various parameters have on the chaotic motion utilizing techniques of dynamical systems. An important factor is the coupling between the orientation and the instantaneous settling velocity. While the various physical parameters have specific relations to the particle aspect ratio of a spheroid [17] it is useful to investigate more general values to determine the essential features of the dynamics. For example this will allow us to consider separately the particle response to flow vorticity and to rate of strain. The equations of particle motion and the flow field are given in Sec. II, introducing both the full three-dimensional problem and the motion restricted to a vertical plane. In Sec. III the latter restricted problem, which involves the particle position in the vertical plane and an orientation angle, is expressed as a three-variable system that matches recent theory developed by Mezic and Wiggins [20] for extended one action—two-angle-variable, volume-preserving differential equations. This allows us to use recent results on volume-preserving maps in determining the persistence of particle suspension and regular motion for spheroidal particles. The restricted problem is further considered in Sec. IV, where the Poincaré sections and values of the Lyapunov exponents show the separate regions of regular and chaotic motion in the flow. Finally, in Sec. V, results for the full, unrestricted motion are discussed.

II. EQUATIONS OF MOTIONS

In this paper we consider the motion of a small axisymmetric particle turning in response to the local velocity gradient and the changes in gravitational settling velocity that occur as the particle turns. As in the paper by Jeffery [13], the particle is assumed to be sufficiently small that the local disturbance flow due to the presence of the particle is a low Reynolds number Stokes flow. The fluid force and torque on the particle are then linearly related to the relative velocity of the particle to the surrounding fluid, the angular velocity, and the local velocity gradient of the imposed flow field. With negligible particle inertia the fluid force balances the resultant force of gravity on the particle and there is no net torque. The motion is described by the set of equations

$$\frac{d\mathbf{x}}{dt} = \mathbf{u}(\mathbf{x}(t),t) + W_1(\hat{\mathbf{g}}\cdot\mathbf{m})\mathbf{m} + W_2(\hat{\mathbf{g}} - (\hat{\mathbf{g}}\cdot\mathbf{m})\mathbf{m}), \quad (1)$$

$$\frac{d\mathbf{m}}{dt} = \frac{1}{2}(\boldsymbol{\omega} + D\mathbf{m}\times\mathbf{E}\cdot\mathbf{m})\times\mathbf{m}. \quad (2)$$

Here $\mathbf{x}$ is the instantaneous position of the center of mass of the axisymmetric particle, $\hat{\mathbf{g}}$ is the unit vector in the direction of gravity, $\mathbf{m}$ is a unit vector aligned with the axis of symmetry that rotates with body, W_1 is the terminal fall speed parallel to $\mathbf{m}$, W_2 is the terminal fall speed perpendicular to $\mathbf{m}$, and $d\mathbf{x}/dt$ is the particle velocity which responds to the local fluid velocity $\mathbf{u}(\mathbf{x}(t),t)$ in the surrounding flow. The orientation changes with the local flow vorticity $\boldsymbol{\omega}$, and $\mathbf{E}$, the rate of strain tensor. D is a parameter that determines the degree to which the particle turns to align with the principal axes of the local rate of strain. For a complete description of the derivation, see Ref. [17].

It is possible to determine the specific values for the parameters W_1, W_2, and D for spheroidal particles in terms of the aspect ratio λ using standard relations [14]. These are

$$W_2/W_1=\frac{[(2\tau^2-1)\ln(\lambda+\tau)+\lambda\tau]}{2[(2\tau^2+1)\ln(\lambda+\tau)-\lambda\tau]}$$

for a prolate spheroid, $\lambda>1$ and $\tau^2=\lambda^2-1$, while for an oblate spheroid, $\lambda<1$ and $\tau^2=1-\lambda^2$

$$W_2/W_1=\frac{[(2\tau^2+1)\tan^{-1}(\tau/\lambda)-\lambda\tau]}{2[(2\tau^2-1)\tan^{-1}(\tau/\lambda)+\lambda\tau]}.$$

Thus for a spheroidally shaped particle $\frac{1}{2}\leqslant W_2/W_1\leqslant\frac{3}{2}$. The values of the parameter D are

$$D=(\lambda^2-1)/(\lambda^2+1).$$

These relations are indicative of the range of values to be expected for an axisymmetric particle though in the results to be presented the parameters W_2/W_1 and D are varied independently.

We examine a particle motion in a two-dimensional cellular flow which is a steady-state solution of the inviscid Euler equations for an incompressible flow, and is chosen because it is encountered in the onset of thermal convection in heated horizontal layers and is also a prototype model for more complex turbulent flows. For a two-dimensional cellular flow given by the stream function $\psi=\pi^{-1}\sin\pi x_1\sin\pi x_2$, the corresponding velocity field in fixed coordinates is

$$\mathbf{u}=(u_1,u_2,0)=(\sin\pi x_1\cos\pi x_2,-\cos\pi x_1\sin\pi x_2,0),$$

and the x_2 axis is aligned vertically, parallel to $\hat{\mathbf{g}}$. Throughout the paper diagrams showing particles settling are drawn with the positive x_2 axis pointing upward on the page, in the usual manner of presenting plots in the (x_1,x_2) plane. The flow is given in dimensionless form, scaled by the maximum vertical velocity and such that the width of a flow cell is unity. These velocity and length scales are used to give all results in dimensionless form. The corresponding vorticity vector is $\boldsymbol{\omega}=(0,0,\omega)$ where $\omega=2\pi\sin\pi x_1\sin\pi x_2$. The rate of strain tensor has two nonzero components $E=E_{11}=-E_{22}$, where $E=\pi\cos\pi x_1\cos\pi x_2$. The equations of motion (1) and (2) for a nonspherical particle take the forms

$$\frac{dx_1}{dt}=u_1+(W_1-W_2)m_1m_2, \tag{3a}$$

$$\frac{dx_2}{dt}=u_2+W_2+(W_1-W_2)m_2^2, \tag{3b}$$

$$\frac{dx_3}{dt}=(W_1-W_2)m_2m_3, \tag{3c}$$

$$\frac{dm_1}{dt}=-\tfrac{1}{2}\omega m_2+DEm_1(m_3^2+2m_2^2), \tag{4a}$$

$$\frac{dm_2}{dt}=\tfrac{1}{2}\omega m_1-DEm_2(m_3^2+2m_1^2) \tag{4b}$$

$$\frac{dm_3}{dt}=DEm_3(m_2^2-m_1^2), \tag{4c}$$

with $m_1^2+m_2^2+m_3^2=1$.

We will first consider a restricted motion, where a particle is oriented in a vertical plane and $m_3=0$. In this case, there is no tendency to turn out of the plane, and we can consider only (x_1,x_2,θ) motion of the particle, where θ specifies the orientation in the plane. We will approach the problem by considering in turn $W_1\neq W_2$ but $D=0$, then $D\neq 0$. The reason for this is that if $D=0$, the system is conservative in phase space and yet retains a coupling of the particle velocity and orientation which seems to be an essential ingredient for a chaotic motion. We will show that setting $D\neq 0$ does not qualitatively change the dynamical results significantly. We will subsequently consider the extension to the full system.

If initially $m_3(t)=0$, then this condition will persist, and the particle remains oriented in a vertical (x_1,x_2) plane. We will first consider this restricted system

$$\frac{dx_1}{dt}=\sin\pi x_1\cos\pi x_2+\Delta W\sin\theta\cos\theta,$$

$$\frac{dx_2}{dt}=-\cos\pi x_1\sin\pi x_2+W+\Delta W\sin^2\theta \tag{5}$$

$$\frac{d\theta}{dt}=\pi\sin\pi x_1\sin\pi x_2-2D\pi\cos\pi x_1\cos\pi x_2\sin\theta\cos\theta.$$

The orientation of the particle in the (x_1,x_2) plane is here specified by the angle θ, $m_1=\cos\theta$, and $m_2=\sin\theta$. The difference in the two settling velocities, W_1-W_2, is represented by ΔW, which may be positive or negative, and the value of W_2 is simply denoted as W.

III. PERSISTENCE OF PERMANENT PARTICLE SUSPENSION

We begin by considering the manner in which the motion of a spheroidal particle differs from that of a spherical one in the cellular flow field, regarding the nonspherical shape as a perturbation. In a vertical plane a spherical particle may be suspended by the flow, as illustrated by Fig. 1, and the particle follows a closed path depending on its position and the value of the settling velocity W. Of special interest is whether or not this suspension and the existence of closed orbits persists for the nonspherical particles. An answer to this question can be given using the recent work of Mezic and Wiggins [20], when the perturbation $\Delta W\neq 0$ is introduced but with the restriction still that $D=0$ in Eqs. (5). With the particle rotating in response only to the local vorticity and not the rate of strain the system of Eqs. (5) is volume preserving in phase space, which is a requirement of the theory [20]. A further requirement of the theory is that the equations of motion be reformulated in terms of action-angle variables and various features of the unperturbed, spherical particle, motion explored.

For a spherical particle, where ΔW and D are both zero system (5) reduces to

$$\frac{dx_1}{dt}=\sin\pi x_1\cos\pi x_2,$$

$$\frac{dx_2}{dt} = -\cos\pi x_1 \sin\pi x_2 + W, \tag{6}$$

$$\frac{d\theta}{dt} = \pi \sin\pi x_1 \sin\pi x_2 .$$

Within the unit cell $\{(x_1,x_2)|0\leqslant x_1,x_2\leqslant 1\}$ there are critical points for the translational motion at $[0,(1/\pi)\sin^{-1}W]$ and $[0,1-(1/\pi)\sin^{-1}W]$ provided $0\leqslant W\leqslant 1$. These are hyperbolic saddle points corresponding to suspension of the particle in a vertical upflow. Another critical point lies at $[(1/\pi)\cos^{-1}W,\frac{1}{2}]$ in the interior of the cell, this point being a center. Particle suspension is only possible if $W\leqslant 1$; otherwise all particles settle out along open trajectories, as also shown in Fig. 1. The bounding trajectory separating the region of closed particle paths from the settling region is formed by the heteroclinic orbit connecting the saddle points. The extent of this suspension region diminishes as W increases [1,2].

Another feature of the translational motion is that along any particle path the quantity

$$H = \frac{1}{\pi}\sin\pi x_1 \sin\pi x_2 - W x_1 \tag{7}$$

is constant. Indeed this modification of the streamfunction ψ forms a Hamiltonian for the motion which may be rewritten as

$$\frac{dx_1}{dt} = \frac{\partial H}{\partial x_2},$$

$$\frac{dx_2}{dt} = -\frac{\partial H}{\partial x_1}, \tag{8}$$

The trajectories are then the level sets of H. Within the suspension region of the unit cell H is positive and is zero on the bounding trajectory. In Fig. 2, level sets of H are shown for $W=0.1$ and 0.4 to illustrate both the closed paths of suspended particles and the open paths of the settling spherical particles. These are given in the domain $\{(x_1,x_2)|0\leqslant x_1,x_2\leqslant 2\}$ for comparison with later results.

For a sphere the particle orientation θ is decoupled, and has no influence on the particle position. At the saddle points the local vorticity is zero and the particle does not rotate, so that at these locations any initial value of θ will give an equilibrium point to system (6). More generally the particle will rotate as it moves along a closed path in the (x_1,x_2) plane. An important feature is the ratio of the relative periods for particle rotation and for the completion of a closed orbit in the (x_1,x_2) plane. In the phase space formed by (x_1,x_2,θ) the motion of a suspended sphere lies on a torus, the closed paths illustrated in Fig. 2 are simply the projections of the torus onto the (x_1,x_2) plane. The complexity of the motion on the torus is determined by the ratio of the two periods. The issue of whether or not a nonspherical particle is suspended depends on the persistence of such tori.

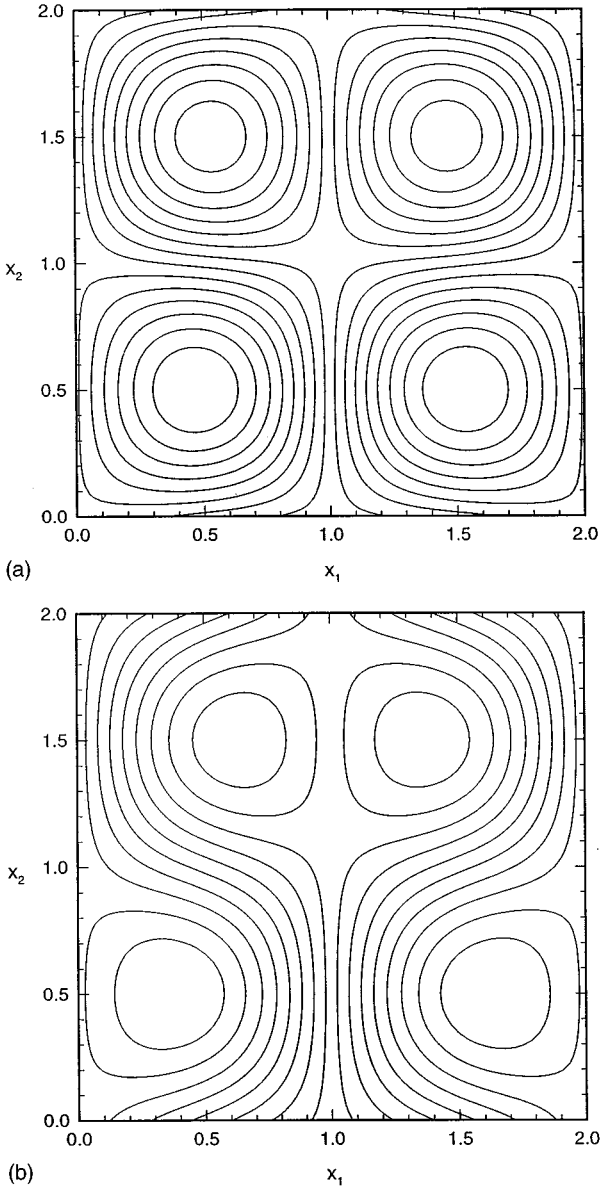

FIG. 2. Level sets of H corresponding spherical particle trajectories in the region $\{(x_1,x_2)|0\leqslant x_1,x_2\leqslant 2\}$; (a) $W=0.1$, and (b) $W=0.4$.

A. Action-angle variables

In order to apply the results of recent theory [20] the unperturbed problem (6), where $\Delta W=0$ and the particle is spherical, must be written in terms of a set of one action, two angle variables. As a first step the system is written in the canonical form

$$dz_1/dt = \partial H/\partial z_2,$$

$$dz_2/dt = -\partial H/\partial z_1, \tag{9}$$

$$dz_3/dt = k_3(z_1,z_2),$$

through the change of variables $(z_1,z_2,z_3)=(x_1,x_2,\theta)$. The action variable I is given by

$$I=\frac{1}{2\pi}\int_{H=h} z_2 dz_1, \tag{10}$$

where the integral is over the level set $H=h$ corresponding to a closed path in the (z_1,z_2) coordinates, and z_2 is specified in terms of z_1 by Eq. (7). The action variable is proportional to the area enclosed by the particle path and is defined in the unit cell for the region where H is positive. The largest positive value of H occurs at the center critical point where

$$H=\frac{1}{\pi}\{(1-W^2)^{1/2}-W\cos^{-1}W\}, \tag{11}$$

at which point I is zero, while I takes its largest negative value for $H=0$. The Hamiltonian and system (9) have a reflexional symmetry about the line defined by $\sin\pi z_2=1$. As a result, action I can be evaluated by integrating between the two values of z_1 at which the level set intersects with $z_2=\frac{1}{2}$. These points, $z_{1\min}$ and $z_{1\max}$ with $0<z_{1\min}\leqslant z_{1\max}<1$, are the two solutions of

$$\pi H+\pi W z_1=\sin\pi z_1. \tag{12}$$

The action variable $I(H)$, for a given value of the parameter W, is thus

$$I(H)=\frac{-1}{\pi}\int_{z_{1\min}}^{z_{1\max}}\left\{1/2-\pi^{-1}\sin^{-1}\left(\frac{\pi(H+Wz_1)}{\sin\pi z_1}\right)\right\}dz_1. \tag{13}$$

The first angle variable α is defined by

$$\alpha=2\pi t/T(H), \tag{14}$$

where $T(H)$ is the period for a closed path in the (z_1,z_2) plane. Again the reflexional symmetry permits us to write down an explicit integral for $T(H)$ as

$$T(H)=2\int_{z_{1\min}}^{z_{1\max}}\frac{dz_1}{\dot{z}_1},$$

where the integral is over the segment of the path $z_2\leqslant\frac{1}{2}$. This integral leads to

$$T(H)=2\int_{z_{1\min}}^{z_{1\max}}\{\sin^2(\pi z_1)-\pi^2(H+Wz_1)^2\}^{-1/2}dz_1. \tag{15}$$

This integral is singular at the two endpoints, and must locally be reformulated as an integral of $1/\dot{z}_2$ with respect to z_2 to obtain numerical values. The change of variables (z_1,z_2) to (I,α) [see, for example, Wiggins [21]] yields the new equations describing the system

$$\dot{I}=0,$$

$$\dot{\alpha}=2\pi/T(H)=\Omega_1(I), \tag{16}$$

$$\dot{z}_3=h_3(I,\alpha)=k_3(z_1(I,\alpha),z_2(I,\alpha)).$$

This first change of variables converts the closed path trajectories of suspended spherical particles in the (z_1,z_2) plane to motion along a circle $I=\text{const}$, and α is a rescaled time variable that changes by 2π for each complete circuit. Numerical results for the dependence of the action variable I and the angular frequency Ω_1 on H are given in Fig. 3 for specific values of W equal to 0.1 and 0.4. The values of I are negative for the counterclockwise orientation of the motion in the unit cell; I has its most negative value along the bounding trajectory where H is zero and vanishes at the center critical point where H is a maximum. The angular frequency increases monotonically too and satisfies the relation $dI/dH=1/\Omega_1$ implied by choice (10).

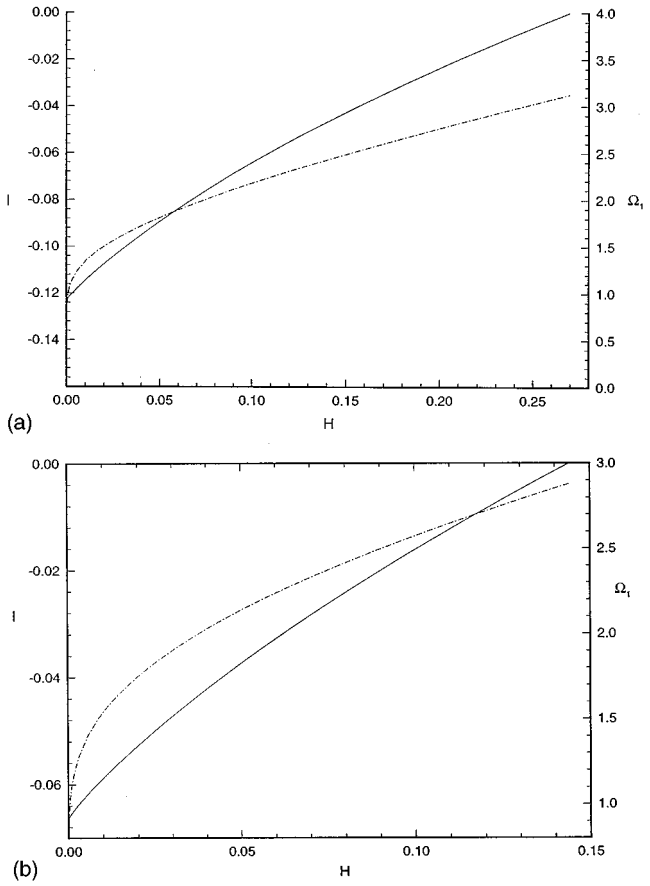

FIG. 3. Variation of the action variable I (solid line) and first angular frequency Ω_1 (broken line) with values of H, $0\leqslant H\leqslant H_{\max}$ given by Eq. (11), for $W=0.1$ and 0.4.

A second change of variables (I,α,z_3) to (I,ϕ_1,ϕ_2) is introduced based on the result (theorem 3.1) of Mezic and Wiggins [20]. This is defined by $(I,\alpha)=(I,\phi_1)$, and the second angle variable ϕ_2 is

$$\phi_2=z_3+\frac{\Delta z_3}{2\pi}\alpha-\int_0^\alpha\frac{h_3(I,\alpha')}{\Omega_1}d\alpha'. \tag{17}$$

The integration in the angle variable α is over a level set of H (or I) for a closed path and Δz_3 is defined as

$$\Delta z_3=\int_0^{2\pi}\frac{h_3(I,\alpha)}{\Omega_1(I)}d\alpha. \tag{18}$$

This is equivalent to a time integral of h_3 over one complete period $T(H)$ of motion in the (z_1,z_2) plane. The value of Δz_3 is the angle θ through which the sphere rotates during

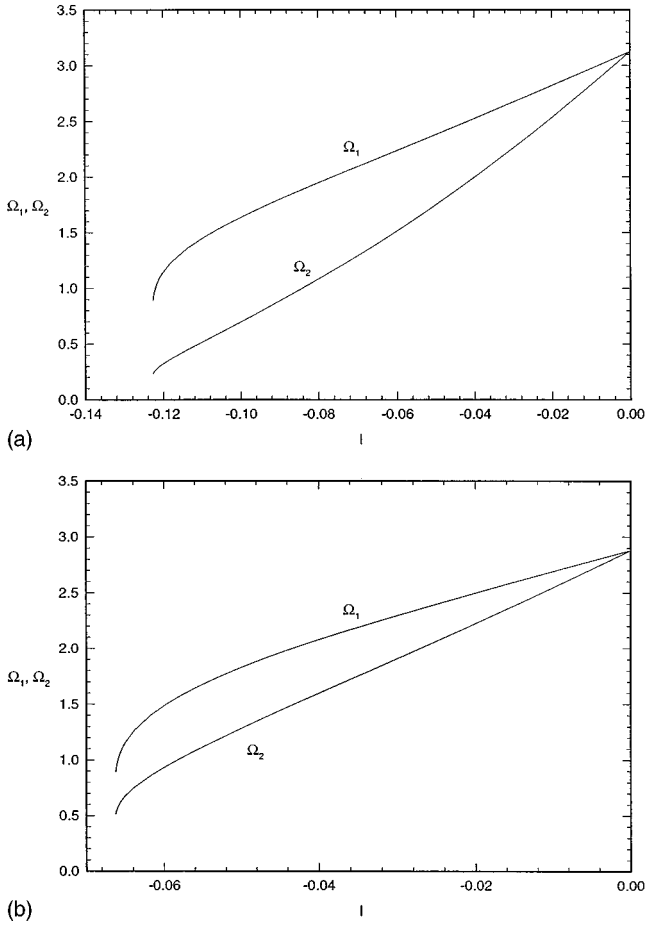

FIG. 4. Angular frequencies Ω_1 and Ω_2 as functions of action I; (a) $W=0.1$ and (b) $W=0.4$.

one such complete period, and this is obviously independent of the chosen starting point on such a closed circuit. In terms of these new variables, the system of equations (6) becomes

$$\dot{I}=0,$$

$$\dot{\phi}_1=\Omega_1(I), \tag{19}$$

$$\dot{\phi}_2=\Omega_2(I)=\frac{\Delta z_3}{2\pi}\Omega_1(I).$$

Formulation (19) shows that in phase space the motion is naturally foliated into a set of two-dimensional tori, determined by the angle variables ϕ_1 and ϕ_2. The structure of the motion on the tori then depends on whether or not the periods or the angular frequencies Ω_1 and Ω_2 are rationally related. If they are not the solution is quasiperiodic and the motion is dense on the torus.

Figure 4 shows numerical values of $\Omega_1(I)$ and $\Omega_2(I)$ evaluated for W equal to 0.1 and 0.4. These are obtained from Eqs. (15) and (18) with due attention to the endpoints $z_{1\min}$ and $z_{1\max}$. A local analysis at the center critical point shows that Ω_1 equals Ω_2 when I is zero, and this is not dependent on the specific value of W provided $0 \leqslant W < 1$. In the special context of W being zero, Eqs. (6) and (7) show that k_3 equals $\pi^2 H$ and is a constant of the motion. In this case $\Omega_2(I)$ is $\pi^2 H(I)$.

B. Volume-preserving perturbation

With formulation (19) we are now able to address the persistence of permanent suspension of slightly nonspherical particles. The perturbations in particle shape are restricted to $D=0$ and $\Delta W \neq 0$, so that the motion is still volume preserving in phase space. The preceding discussion has shown that the permanent suspension of a particle in the vertical (x_1, x_2) plane is equivalent to the persistence of tori in the phase space as the perturbation is introduced.

The original set of equations (5) may be expressed in terms of a perturbation of system (19). Following Eq. (9), this is

$$\frac{dz_1}{dt}=\frac{\partial H}{\partial z_2}+\Delta W \sin z_3 \cos z_3,$$

$$\frac{dz_2}{dt}=-\frac{\partial H}{\partial z_1}+\Delta W \sin^2 z_3, \tag{20}$$

$$\frac{dz_3}{dt}=k_3(z_1,z_2)=\pi \sin \pi z_1 \sin \pi z_2,$$

and hence, in terms of the action-angle variables,

$$\dot{I}=\Delta W F_0(I,\phi_1,\phi_2),$$

$$\dot{\phi}_1=\Omega_1(I)+\Delta W F_1(I,\phi_1,\phi_2), \tag{21}$$

$$\dot{\phi}_2=\Omega_2(I)+\Delta W F_2(I,\phi_1,\phi_2).$$

Mezic and Wiggins [20] demonstrated how the first variation in ΔW of Eq. (21) about the unperturbed system (19) may be used to generate a volume-preserving, three-dimensional map by integrating the perturbed motion over a specified time interval τ. The perturbations in this context are time independent, and the system is autonomous. The simple nature of the unperturbed problem (19) means that his procedure may be done explicitly; see the Appendix. At this point recent results [22] for KAM-type theories for volume-preserving maps in three dimensions may be applied. Under the conditions of the theorem of Cheng and Sun [22], as given by Mezic and Wiggins [20] in theorem 5.1, there is a nontrivial interval for ΔW about $\Delta W=0$ for which the perturbed system admits a family of invariant tori. Further there is a Cantor set, with increasing measure as $|\Delta W| \to 0$, such that if the value of I is a member of the set there is a corresponding invariant torus. An invariant torus of the map then corresponds to a regular particle trajectory in physical space with the particle permanently suspended.

The development and application of KAM-type theories to odd dimensional systems is nontrivial and has a quite different character to standard KAM theory. Feingold, Kadanoff, and Piro [23], Cheng and Sun [22], and Xia [24] all contributed to this work on three-dimensional, volume-preserving diffeomorphisms that may be characterized as having only one slowly varying action variable. While it is possible to consider whether Ω_1 and Ω_2 are rationally related or not, or give strongly irrational rotation numbers, this is not of itself sufficient in a three-dimensional system to determine the persistence of invariant tori. Xia [24] extended the theory to higher dimensions.

As summarized in the Appendix, the three-dimensional map derived from the perturbed equations of motion is

$$I' = I + \Delta W \widetilde{F}_0(I,\phi_1,\phi_2) + O(\Delta W^2),$$

$$\phi_1' = \phi_1 + \Omega_1(I) + \Delta W \widetilde{F}_1(I,\phi_1,\phi_2) + O(\Delta W^2), \quad (22)$$

$$\phi_2' = \phi_2 + \Omega_2(I) + \Delta W \widetilde{F}_2(I,\phi_1,\phi_2) + O(\Delta W^2);$$

the time interval $\tau = 1$ gives a period-1 map. At this point we depart from the earlier methods [20,22] and prefer to use the result of Xia [24], which is easier to apply in this context. The requirements for the theorem on the existence of invariant tori of map (22) are that $\widetilde{F}_0$, $\widetilde{F}_1$, and $\widetilde{F}_2$ are real analytic functions in their arguments. The map is volume preserving, as the original differential equations are, and this property is preserved by the perturbation expansion and integration. Finally we also require that Ω_1 and Ω_2 satisfy a nondegeneracy condition

$$Q \equiv \begin{vmatrix} \Omega_1'(I) & \Omega_2'(I) \\ \Omega_1'' & \Omega_2''(I) \end{vmatrix} \geqslant d > 0. \quad (23)$$

The above determinant Q, based on the derivatives of Ω_1 and Ω_2, must be positive and bounded away from zero by some positive number d.

In previous treatments [20,22], the time intervals were rescaled to give $\Omega_1 = I$, and a single condition on $\Omega_2''(I)$ was imposed. While convenient for developing theorems, this is not helpful for the practical verification of the conditions. Simple manipulation, on the other hand, shows that

$$d/dI(\Omega_2'/\Omega_1') = Q/\Omega_1'^2. \quad (24)$$

It is thus sufficient to show $d/dI(d\Omega_2/d\Omega_1)$ is strictly positive and bounded away from zero, or, provided that $\Omega_1' > 0$, that

$$d/d\Omega_1(d\Omega_2/d\Omega_1) \geqslant p > 0 \quad (25)$$

for some positive number p. Referring back to the numerical results of Figs. 3 and 4, we may clearly see that $d\Omega_1/dI$ is indeed strictly positive. In Fig. 5 the numerical data have been refined and accurately matched to an interpolating function to give Ω_2 as a function of Ω_1. From this interpolating function, first and second derivatives of Ω_2 with respect to Ω_1 have been evaluated. The numerical values show, as expected, a smooth continuous variation and this is not altered by increased resolution. Condition (25) is clearly seen to be satisfied in the two cases $W = 0.1$ and 0.4. It has also been verified in other cases.

The discussion of this section thus demonstrates that permanent suspension of nonspherical particles is still to be expected in the context of $D = 0$, where there is coupling of particle orientation to the local vorticity but not to the local rate of strain. The numerical results of the following section show that suspension occurs too in the more general case with $D \neq 0$.

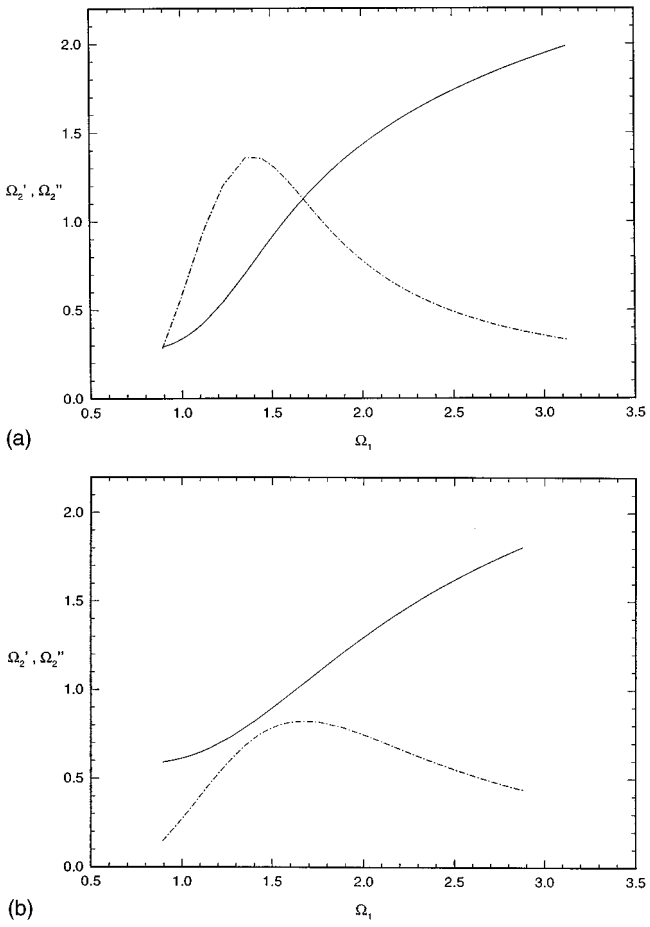

FIG. 5. First and second derivatives $d\Omega_2/d\Omega_1$ (solid line) and $d^2\Omega_2/d\Omega_1^2$ (broken line), as functions of Ω_1; (a) $W = 0.1$, and (b) $W = 0.4$.

IV. REGULAR AND CHAOTIC MOTION

The more general features of nonspherical particle motion, restricted to a vertical plane as given by Eq. (5), are investigated using Poincaré sections and numerical calculations of the Lyapunov exponents. Poincaré sections in the (x_1, x_2) plane of the system are constructed by taking the values x_1 and x_2 given by the intersections with $\sin\theta = 0$. The equations of motion (5) are periodic in the orientation angle θ, with a period π, corresponding to the symmetry of a spheroidal particle. The system is periodic too in the variables x_1 and x_2 and values of these are mapped back, modulo 2, to the interval [0,2]. A Runge-Kutta fourth-order numerical scheme with a fixed time step size of 10^{-3} has been used for the integration of the system, and Henon's [25] method is adopted to obtain the sections. A typical Poincaré section for a spherical particle, corresponding to the unperturbed system (6), is shown in Fig. 6 with $W = 0.1$. The sections, generated by ten particles initially introduced in the unit cell $\{(x_1, x_2) | 0 \leqslant x_1, x_2 \leqslant 1\}$, show clearly the regularity of the motion and the separate regions of permanent particle suspension and particle settling. These may be compared with the similar particle trajectories and level sets shown in Fig. 2.

Figure 7 shows a typical Poincaré section produced by the perturbed system of the form described in Sec. III. Here $W = 0.1$ and $\Delta W = 0.2$ while D is zero. Three distinct types of motion are observable: regular motion of suspended par-

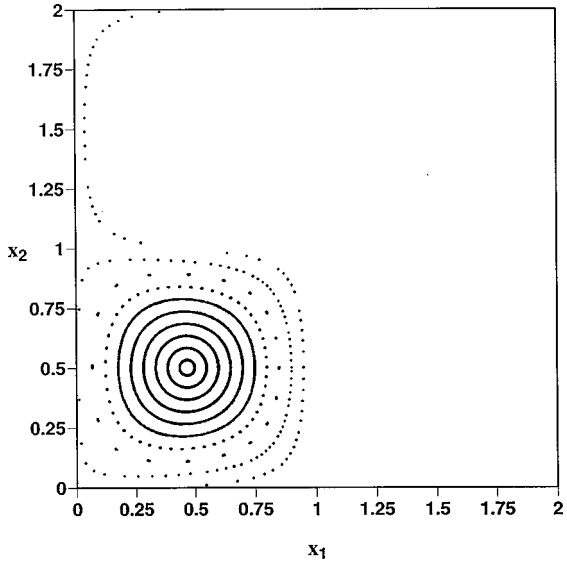

FIG. 6. Poincaré section at $\sin\theta=0$ when $D=0.0$, $W=0.1$, and $\Delta W=0$.

ticles, regular motion of settling particles and chaotic motion of settling particles. The regular motion, suspended or settling, is analogous to that of the spherical particles shown in the Poincaré sections of Fig. 6. The particle-suspending region in the Poincaré section is composed of closed curves defined by different initial conditions of a particle, and is seen in the lower left side of the figure. An enlarged version of this region is shown in Fig. 7(b). The chaotic region observed in Fig. 7(a) is produced by three different particle trajectories. To verify that the region is indeed chaotic, we compute the Lyapunov exponents along a solution starting at a selected point in the region. The largest Lyapunov exponent for the solution starting at the point (0.1, 0.1, 0.0) converges to the positive value of 0.53. The other two exponents converge to zero and to -0.53.

The sum of the Lyapunov exponents should be zero, since system (20) is volume preserving in phase space. That the second exponent is zero should be expected too (see Haken [26]), as the governing differential equations (20) are autonomous. For a general autonomous system of the form

$$\dot{\mathbf{z}}=\mathbf{f}(\mathbf{z}),$$

the equation governing the linear variation $\delta\mathbf{z}$ used in the computation of Lyapunov exponents is

$$d/dt(\delta z_i)=\delta z_j \partial f_i/\partial z_j,$$

evaluated along the path $\mathbf{z}(t)$. The results depend on the initial point $\mathbf{z}(0)$, and the exponents are calculated as

$$\lambda=\lim_{t\to\infty}\frac{1}{t}\ln[\|\delta\mathbf{z}(t)\|/\|\delta\mathbf{z}(0)\|].$$

An orthogonalization procedure is used to select the principal directions for $\delta\mathbf{z}(0)$ needed to obtain the second and third exponents. For the autonomous system (20), an initial variation tangent to the solution path yields the solution

$$\delta\mathbf{z}(t)=\mathbf{f}(\mathbf{z}(t))[\|\delta\mathbf{z}(0)\|/\|\mathbf{f}(\mathbf{z}(0))\|],$$

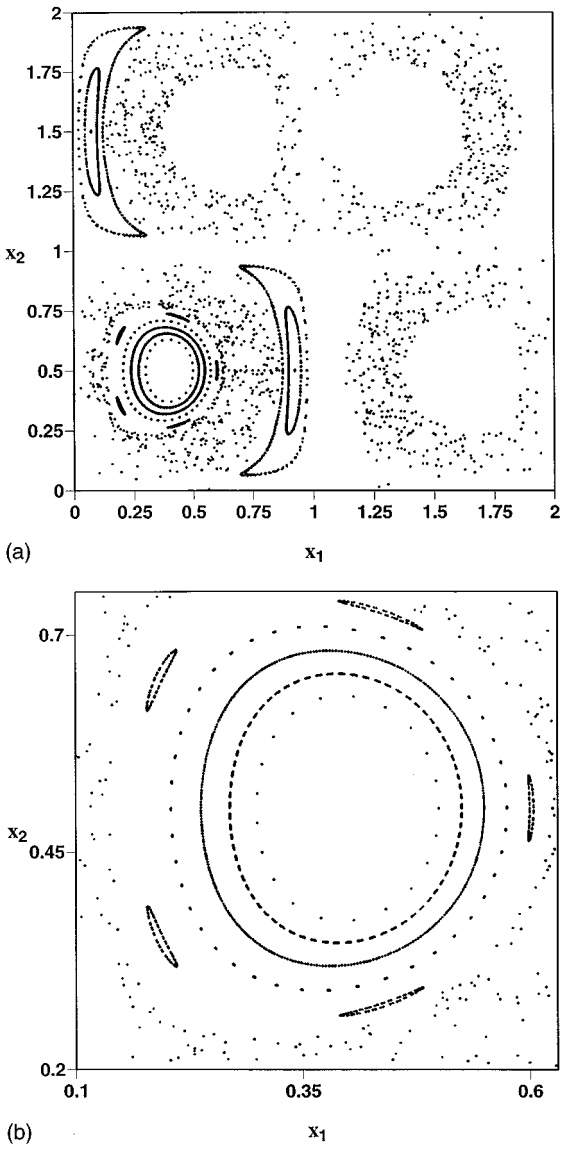

FIG. 7. (a) Poincaré section at $\sin\theta=0$ when $D=0.0$, $W=0.1$, and $\Delta W=0.2$; and (b) the closeup of the particle-suspending region.

that remains tangent to the path $\mathbf{z}(t)$. This solution gives one of the principal directions and yields one of the Lyapunov exponents. For Eq. (20) the Euclidean norm of $\mathbf{f}$ is bounded and is in general nonzero. In the long-term limit, then, the exponent for this variation is zero.

We have computed the largest Lyapunov exponents for several solutions starting at different initial conditions in the chaotic region. Table I shows the results, which further confirm the chaotic nature of the motion. We may conclude that the Lyapunov exponents are dependent on the initial starting points even if we take into account numerical errors and the inability to take an infinitely long time interval.

The structure of the regular particle motion in the settling region shown in the Poincaré section of Fig. 7 is given by the composition of crescent-shaped patterns, one in the upper part of the figure to the left and the other in the lower part between about $x_1=0.8$ and 1.0. The particles continuously settle, alternately generating section data points on one of the lower crescents and a corresponding upper crescent, in the

TABLE I. The list of the largest Lyapunov exponents when $D=0.0$, $W_1=0.3$, and $W_2=0.1$.

Initial points	Largest Lyapunov exponents
$(x_1=0.1,\ x_2=0.1,\ x_3=0.0)$	0.53
$(x_1=0.3,\ x_2=0.2,\ x_3=0.0)$	0.52
$(x_1=0.7,\ x_2=0.3,\ x_3=0.0)$	0.66
$(x_1=0.5,\ x_2=0.5,\ x_3=0.0)$	0.66
$(x_1=0.7,\ x_2=0.5,\ x_3=0.0)$	0.62
$(x_1=0.6,\ x_2=0.8,\ x_3=0.0)$	0.64

direction of x_2 increasing. Each upper crescent and the corresponding lower one is produced by a single-particle trajectory starting at a given initial position. The feature of regular settling motion was not observed in the earlier study of Mallier and Maxey [17], and only become apparent in this more careful investigation. A numerical calculation of the Lyapunov exponents for particles in these crescent regions shows that the exponents all converge to zero in the long term, confirming the regular nature of the motion there.

Comparison of systems (20) and (6) shows that Eq. (20) has discrete fixed points, whereas Eq. (6) has an infinite number of them. This change implies the breakdown of a two-dimensional invariant surface that separates a particle-suspending region from a particle-settling region, such as is observed when we study Eq. (6), under perturbation via ΔW. This would account for the emergence of chaotic motion for system (20). Since system (20) is volume preserving, it would not have any kind of attractor. Thus a particle that initially starts in a chaotic region would remain in the region visiting every part of the region. The survival of a particle-suspending region is to be expected from the results in Sec. III. Note that this region of permanent particle suspension does not extend to the cell boundary at $x_1=0$, unlike that of the spherical particles shown in Fig. 6 and illustrated in Fig. 2. Near this cell boundary the vertical flow velocity counteracting particle settling is strongest. The effect of the perturbation ΔW is to reduce the extent of the region for particle suspension.

We restate the fully perturbed system, where not only the effect of the gravitational settling is included but also the coupling of the particle orientation to the local rate of strain

$$\frac{dx_1}{dt}=\sin\pi x_1\cos\pi x_2+\Delta W\sin\theta\,\cos\theta,$$

$$\frac{dx_2}{dt}=-\cos\pi x_1\sin\pi x_2+W+\Delta W\sin^2\theta, \tag{26}$$

$$\frac{d\theta}{dt}=\pi\,\sin\pi x_1\sin\pi x_2-2D\pi\,\cos\pi x_1\cos\pi x_2\sin\theta\,\cos\theta.$$

We should note that system (26) is neither volume preserving nor dissipative since the divergence of the vector field is $-2D\pi\,\cos\pi x_1\cos\pi x_2\cos 2\theta$, which may be both positive or negative.

Even with the additional rate-of-strain term, a typical Poincaré section for system (26) does not greatly differ from a typical Poincaré section for Eq. (20). Figure 8 shows a

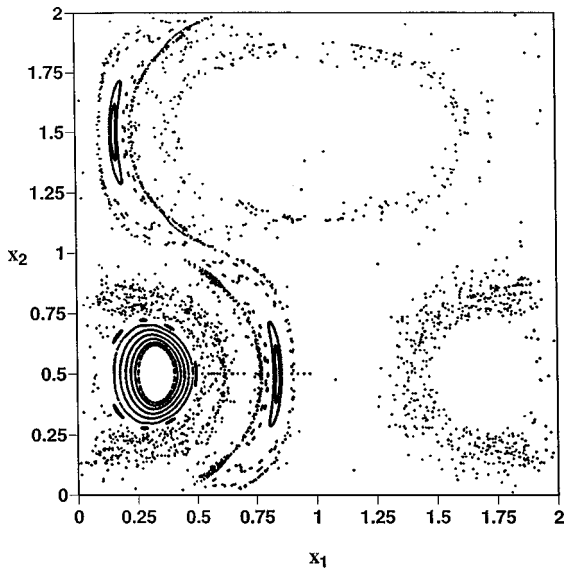

FIG. 8. Poincaré section at $\sin\theta=0$ when $D=0.5$, $W=0.4$, and $\Delta W=0.1$.

Poincaré section constructed with $D=0.5$ and the parameters $W=0.4$ and $\Delta W=0.1$. Both Figs. 7 and 8 show a region of regular particle motion where the particles are suspended permanently. The extent of this region in Fig. 8 is smaller, because of the larger value of W. A region of regular particle settling is observed too, again these sections have a crescent-shaped pattern. The Lyapunov exponents for particle trajectories corresponding to these two regions are all zero. Figure 8 shows further a third region of chaotic motion that is more extensive than in Fig. 7. Table II lists the computed Lyapunov exponents taken along sample solutions which start at different points within the chaotic region. These positive exponent values verify that the region is indeed chaotic. The table also illustrates that the exponents are solution dependent for system (26).

Whether the sum of the Lyapunov exponents of the system at given parameter values is positive, zero, or negative raises an interesting question, since system (26) is neither volume preserving or dissipative. A Lyapunov exponent of order p, $\sigma^{(p)}(\mathbf{x}_0,V_p)$, where $\mathbf{x}_0$ is the initial position and V_p is the volume of a p-dimensional parallelepiped with edges $\mathbf{w}_1,\mathbf{w}_2,\ldots,\mathbf{w}_p$, is

$$\sigma^p(\mathbf{x}_0,V_p)=\lim_{t\to\infty}\frac{1}{t}\ln\frac{\|V_p(\mathbf{x}_0,t)\|}{\|V_p(\mathbf{x}_0,0)\|}.$$

According to Oseledec [27] and Bennettin *et al.* [28], $\sigma^{(p)}$ is the sum of the p largest Lyapunov exponents

TABLE II. The list of the largest Lyapunov exponents when $D=0.5$, $W_1=0.5$, and $W_2=0.4$.

Initial points	Largest Lyapunov exponents
$(x_1=0.3,\ x_2=0.15,\ x_3=0.0)$	0.40
$(x_1=0.6,\ x_2=0.3,\ x_3=0.0)$	0.44
$(x_1=0.7,\ x_2=0.55,\ x_3=0.0)$	0.46
$(x_1=0.4,\ x_2=0.8,\ x_3=0.0)$	0.50

$$\sigma^{(p)}=\sigma_1+\sigma_2+\cdots+\sigma_p$$

for almost all initial V_p's. The relationship between the sum of the Lyapunov exponents and the expansion or contraction of the volume of the system is then

$$\|V_p(t)\|\approx\|V_p(0)\|e^{t\sigma^{(3)}}, \tag{27}$$

where $V_p(t)$ is the volume evolution through time. The case where $\sigma^{(3)}$ is positive should be eliminated on the grounds that a volume cannot expand forever in a bounded space such as the space where system (26) is defined. Thus $\sigma^{(3)}$, the sum of the Lyapunov exponents, must be negative or zero for the system (26) in a chaotic region for all ranges of the values of the parameters. Obviously for regular motion in non-chaotic regions $\sigma^{(3)}=0$. A net reduction in volume, corresponding to the decrease of infinitesimal volumes governed by relationship (27), will occur when $\sigma^{(3)}$ is negative. Calculations for several of the chaotic trajectories illustrated in Fig. 9 give sample values of $\sigma^{(3)}$ equal to zero or -0.00215 and -0.00268. Within the precision of these calculations it is clear that negative values of $\sigma^{(3)}$ do arise. There is no consistent trend for all chaotic particle motion as the system is not ergodic, and the set of Lyapunov exponent values varies with the initial conditions of the particle trajectory.

A tendency toward negative values of $\sigma^{(3)}$ is consistent with the physical characteristics of the particle motion. When D is nonzero, a particle will turn tending to align itself with the local principal axes for the strain rate of the flow. This will restrict the range of possible particle orientations in phase space.

V. GENERAL MOTION

We now consider the general system of equations (3) and (4), where the motion is no longer restricted to a vertical plane and a particle is free to move in three dimensions with arbitrary orientation. As done previously, the two contexts of $D=0$ and $D\neq 0$, are considered separately, corresponding to whether or not the particle orientation is coupled to the local rate of strain. As the Poincaré sections of Sec. IV have shown, a coupling of the particle orientation to the translational motion is the essential ingredient for chaotic motion. This occurs as a nonspherical particle $\Delta W\neq 0$ turns in response to the local vorticity. The additional coupling to the rate of strain by nonzero values of D does not dramatically alter this behavior, at least for the restricted motion in a vertical plane.

A. $D=0$

In the absence of coupling to the local rate of strain in Eq. (4), the system of equations may be simplified significantly. For the two-dimensional cellular flow there is no component of vorticity that would alter the value of the symmetry vector component m_3 in Eq. (4c). As a result m_3 is a constant, be it nonzero or zero. As the vector **m** has unit size it follows that throughout the motion

$$(m_1^2+m_2^2=1-m_3^2=\alpha^2)=\text{const.} \tag{28}$$

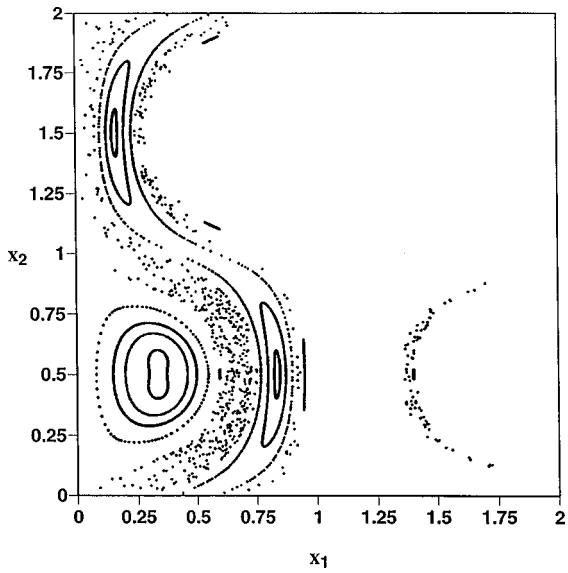

FIG. 9. Poincaré section of the general motion at $\sin\hat{\theta}=0$ for $D=0$, $W=0.4$, and $\Delta W=0.1$; the section is projected onto the (x_1,x_2) plane.

The values of the components m_1,m_2 are restricted to be $0\leqslant m_1,m_2\leqslant\alpha\leqslant 1$ and the particle moves with a fixed angle relative to the vertical plane. A new orientation angle $\hat{\theta}$ may be defined for m_1,m_2, giving the particle orientation as projected onto a vertical plane:

$$m_1=\alpha\cos\hat{\theta},$$

$$m_2=\alpha\sin\hat{\theta}. \tag{29}$$

The other equations (4a) and (4b), governing the particle orientation, simply imply a rotation of $\hat{\theta}$ in response to the local vorticity,

$$\frac{d\hat{\theta}}{dt}=\pi\sin\pi x_1\sin\pi x_2. \tag{30}$$

Beyond this, Eq. (3), governing the particle position, may be written in terms of $\hat{\theta}$ in a manner analogous to Eq. (5),

$$\frac{dx_1}{dt}=\sin\pi x_1\cos\pi x_2+\alpha^2\Delta W\cos\hat{\theta}\sin\hat{\theta},$$

$$\frac{dx_2}{dt}=-\cos\pi x_1\sin\pi x_2+W+\alpha^2\Delta W\sin^2\hat{\theta}, \tag{31}$$

$$\frac{dx_3}{dt}=\alpha(1-\alpha^2)^{1/2}\Delta W\sin\hat{\theta}.$$

A comparison of Eqs. (31) for x_1 and x_2 with the corresponding Eqs. (5) shows that the two sets are identical if the value of ΔW in Eqs. (5) is replaced by the scaled value $\alpha^2\Delta W$. The rotation of $\hat{\theta}$ matches Eqs. (5) too. The third coordinate x_3 has no effect on the other variables, and changes passively in response to the changing orientation. Changes in the displacement x_3 are due solely to the compo-

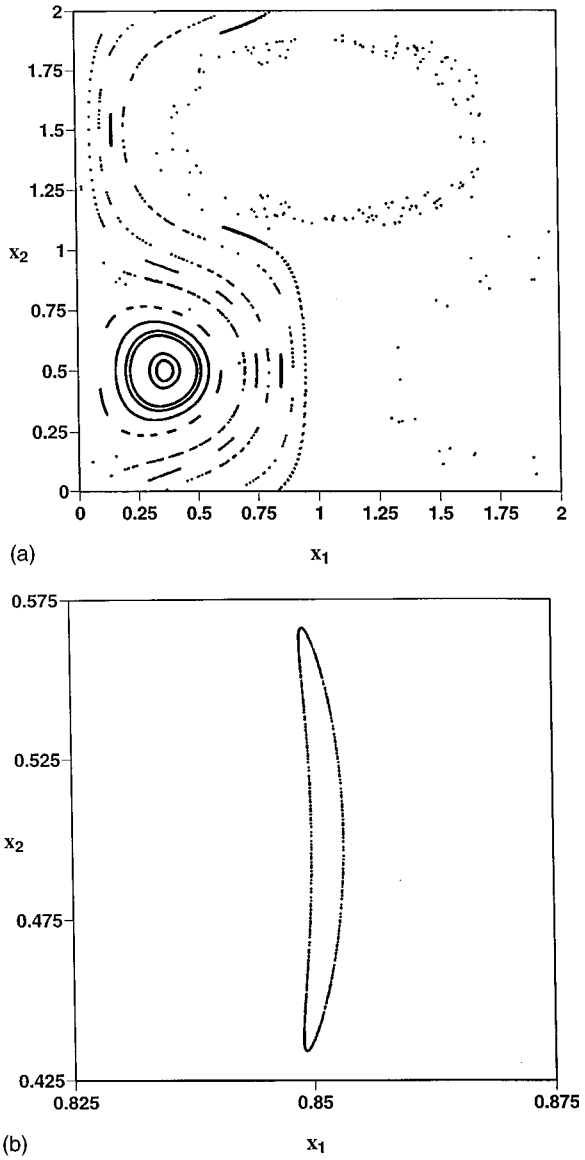

FIG. 10. Poincaré section of the general motion at $\sin\theta=0$ for $D=0.5$, $W=0.4$, and $\Delta W=0.1$, projected onto the (x_1,x_2) plane: (a) full view; (b) a close-up view in the regular settling region.

nent of the settling velocity of a nonspherical particle directed out of the vertical plane.

If the general motion, for $D=0$, is projected onto the (x_1,x_2) plane the system of equations (30) and (31) is entirely equivalent to the previously described motion confined to a vertical plane, but with a reduced value of ΔW. The persistence of regular motion with particle suspension and of regions of regular settling motion are to be expected then in this more general context. This demonstrates too the more general significance of the previous results. Different initial values of m_3 will lead to different results, but as $0\leqslant\alpha\leqslant 1$ and $\alpha^2\Delta W$ controls the degree to which the nonspherical shape affects the motion, the regions of regular motion for suspension or settling will always be at least as large as those given previously for the same value of ΔW.

These observations are supported by numerical results. Figure 9 shows a Poincaré section of this general motion for $D=0$, where the section, taken at $\sin\hat{\theta}=0$, has been projected onto the (x_1,x_2) plane. The settling velocity parameters W and ΔW are 0.4 and 0.1, respectively. The initial value of m_3 is 0.941, so that the value of α is 0.339 and the effective value of the perturbation, $\alpha^2\Delta W$ equals 0.0115. The resulting Poincaré section is very similar to that of Fig. 7, with clearly discernible regions of regular particle suspension, regular settling and chaotic settling. The relatively low value of the effective perturbation gives a larger region of regular particle suspension extending further toward the cell boundary at $x_1=0$. The crescent patterns associated with the regular settling lie in a fairly well-defined ''channel'' and the chaotic motion occurring in the intervening region.

B. $D\neq 0$

In the most general cuontext where the coupling to the rate of strain in three dimensions is included and D is nonzero then no major simplification of Eqs. (3) and (4) is possible. The previously obtained results still provide useful indications as to the typical particle motion. The third coordinate x_3, for displacement out of the vertical plane, still has no influence on the other variables, and simply responds passively to the changing particle orientation. The projection of the motion onto the vertical (x_1,x_2) plane is the most significant. The orientation of the symmetry axis **m** is still strongly governed by the local vorticity, but the coupling to the rate of strain causes the m_3 component to vary continuously. The unit vector **m** can be expressed in terms of two angle variables θ and ϕ with **m** equal to $(\sin\phi\cos\theta,\sin\phi\sin\theta,\cos\phi)$. The rotation (4) of **m** is given by the two evolutionary equations for θ and ϕ as

$$\frac{d\theta}{dt}=\pi\sin\pi x_1\sin\pi x_2-DE(x_1,x_2)\sin 2\theta,$$
$$\frac{d\phi}{dt}=\frac{1}{2}DE(x_1,x_2)\sin 2\phi\cos 2\theta. \tag{32}$$

When $\phi=\pi/2$, m_3 is zero, and the equation for θ is the same as Eq. (26c). If D is zero then ϕ is constant, and the result matches Eq. (30).

Poincaré sections are obtained for the system (x_1,x_2,θ,ϕ), taken at $\sin\theta=0$, and projected onto the (x_1,x_2) plane, with no distinction made as to the value of ϕ. A Poincaré section is shown in Fig. 10 for $D=0.5$, and again the values of W and ΔW are 0.4 and 0.1, respectively. The same general features are observed as before. In the projected Poincaré section of Fig. 10(a), there is a region of regular motion, approximately centered on $x_2=0.5$ and $0.25<x_1<0.5$, where the data points correspond to particles permanently suspended by the flow within the original cell into which they were introduced. There is also a portion of the section showing a chaotic settling motion, and, somewhat harder to distinguish, a region of regular settling motion. However, an enlargement of a portion of the Poincaré section, shown in Fig. 10(b), shows clearly the characteristic crescent-shaped pattern of data points similar to those seen previously in Figs. 7 and 10. As before, the particles settle continuously in a quasiperiodic motion, generating data points in the section alternately on the crescent pattern in the lower and upper cells.

Numerical results for some of the Lyapunov exponents have been calculated for the same conditions of $D=0.5$, $W=0.4$, and $\Delta W=0.1$. A particle introduced at $\mathbf{x}=(0.8,0.5,0.0)$ with orientation $\mathbf{m}=(0.339,0,0.941)$ lies within the region of regular settling motion, and the largest Lyapunov exponent indeed converges to zero. A particle introduced with the same initial conditions, but with $x_1=0.65$, settles chaotically. The largest Lyapunov exponent for this particle is 0.39.

VI. CONCLUSION

The results in this paper illustrate the structural features of the motion of nonspherical particles settling in a steady, nonuniform flow. The possibilities of regular motion with particles suspended by the flow or settling out, together with chaotic settling are all demonstrated. The persistence of regular settling had not been previously observed in earlier work [17]. The independent variation of the parameters ΔW and D confirms that the key ingredient for the chaotic tumbling motion is the coupling of particle orientation to the settling velocity, and the rotation of the particle in response to the changing local vorticity as it settles in the nonuniform flow. The inclusion of the coupling of the orientation to the rate of strain in the presence of vorticity does not significantly alter the results. While these results have been derived for a periodic cellular flow system the same principles should apply in other nonuniform shear flows, and similar features should be observable in shear layers or jet flows. The basic requirement is that there be a circulatory motion in a vertical plane with a nonuniform distribution of horizontal vorticity.

The theoretical arguments presented to demonstrate the persistence of particle suspension are an application of the theory of Mezic and Wiggins [20] for systems of one-action and two-angle variables. In the process of verifying the conditions for the theory an alternative formulation is applied for the nondegeneracy condition. This is easier to use, and may be more readily applied to computational results. Extensions of Hamiltonian theory to systems that are volume preserving in phase space have a number of applications to mixing in fluid flow systems and the dynamics of particle transport. Recent work in this area includes the paper by Cartwright, Feingold, and Piro [29].

In the earlier study by Mallier and Maxey [17] specific aspect ratios of spheroidal particles were used to set values of D, W, and ΔW and to determine the overall features of the motion. For example a prolate spheroid with aspect ratio $\lambda=2$ the value of D is 0.6, and the relative value of ΔW is approximately $0.15W$. For $W=0.24$, about 40% of particles initially distributed uniformly in a unit cell will be permanently suspended, as compared to between 58% and 55% for spherical particles with settling velocities equal to W or $W+\Delta W$, respectively. Similarly if $W=0.48$ or 0.72 about 22% or 8.5% of the particles are retained compared to a range of 35–30% and 17–11% for spherical particles. The nonspherical shape reduces the particle retention below the level that would be expected for a spherical particle even at the higher terminal velocity $W+\Delta W$. Departures from a spherical shape were found also to increase the average particle settling velocity.

Finally, the chaotic tumbling is potentially an important mechanism for the dispersion of small, nonspherical particles settling under gravity. Previously Brenner [30,31] and Dill and Brenner [32] demonstrated that small particles subject to Brownian motion will be dispersed in the horizontal direction. This is due to the dependence of settling velocity on orientation, and the horizontal motion of particles not aligned with the vertical. Under the influence of Brownian motion these particles have a random orientation that gives rise to a Taylor dispersion coefficient significantly greater than that due to translational Brownian motion. Brownian motion is only appreciable for very small particles, 5 μm in diameter in air for example, and even smaller in liquid flows. Chaotic mixing in a nonuniform shear flow by contrast should be effective over a wide range of scales and especially for larger particles. This chaotic dispersion of nonspherical particles even in a steady laminar flow will have similarities to the chaotic dispersion of heavy, inertial particles studied by Crisanti *et al.* [5] and Wang *et al.* [33].

ACKNOWLEDGMENTS

The authors would like to thank Professor Tasso Kaper and Professor Igor Mezic for their helpful comments and suggestions. Support for this work by a DARPA-URI grant, ONR-N00014-86-K0754, with additional support from the National Science Foundation under Grant No. CTS-9424169, is gratefully acknowledged.

APPENDIX: CONSTRUCTION OF THE MAP

The perturbed system of differential equations (20) in terms of (z_1,z_2,z_3) is

$$\begin{aligned} dz_1/dt &= f_1(z_1,z_2)+\Delta W g_1(z_3),\\ dz_2/dt &= f_2(z_1,z_2)+\Delta W g_2(z_3),\\ dz_3/dt &= f_3(z_1,z_2), \end{aligned} \tag{A1}$$

where the functions are defined as

$$\begin{aligned} f_1 &= \sin\pi z_1\cos\pi z_2,\\ f_2 &= -\cos\pi z_1\sin\pi z_2+W,\\ f_3 &= \pi\,\sin\pi z_1\sin\pi z_2,\\ g_1 &= \sin z_3\cos z_3,\\ g_2 &= \sin^2 z_3. \end{aligned} \tag{A2}$$

Within the region of spherical particle suspension, $H>0$, the change of variables from (z_1,z_2,z_3) to (I,ϕ_1,ϕ_2) given by Eqs. (10)–(18) is well defined and a particular pair of values of z_1,z_2 will lie on some level set of H. The angle variables $\phi_1\phi_2$ determine the position on the level set and the particle orientation. The variables z_1,z_2,z_3 may then be expressed as functions of I,ϕ_1, and ϕ_2. An application of the chain rule gives the corresponding differential equations

$$\begin{bmatrix} \dot{I} \\ \dot{\phi}_1 \\ \dot{\phi}_2 \end{bmatrix} = \begin{bmatrix} \partial I/\partial z_1 & \partial I/\partial z_2 & 0 \\ \partial \phi_1/\partial z_1 & \partial \phi_1/\partial z_2 & 0 \\ \partial \phi_2/\partial z_1 & \partial \phi_2/\partial z_2 & \partial \phi_2/\partial z_3 \end{bmatrix} \begin{bmatrix} f_1+\Delta W g_1 \\ f_2+\Delta W g_2 \\ f_3 \end{bmatrix} \tag{A3}$$

These may be written in the more compact form (21),

$$\begin{aligned} \dot{I} &= \Delta W F_0(I,\phi_1,\phi_2), \\ \dot{\phi}_1 &= \Omega_1(I)+\Delta W F_1(I,\phi_1,\phi_2), \\ \dot{\phi}_2 &= \Omega_2(I)+\Delta W F_2(I,\phi_1,\phi_2). \end{aligned} \tag{A4}$$

The construction of the iterated map follows Mezic and Wiggins [20] and begins with a regular perturbation expansion for the motion I,ϕ_1,ϕ_2 for small values of ΔW valid for times of $O(1)$. Thus with the initial values ϕ_1^0 and ϕ_2^2 of the angle variables,

$$\begin{aligned} I^{\Delta W}(t) &= I^0+\Delta W I^1(t)+O[(\Delta W)^2] \\ \phi_1^{\Delta W}(t) &= \phi_1^0+\Omega_1(I^0)t+\Delta W\phi_1^1(t)+O[(\Delta W)^2] \\ \phi_2^{\Delta W}(t) &= \phi_2^0+\Omega_2(I^0)t+\Delta W\phi_2^1(t)+O[(\Delta jW)^2]. \end{aligned} \tag{A5}$$

The functions $I^1(t),\phi_1^1(t)$, and $\phi_2^1(t)$ satisfy the variational equations

$$\begin{aligned} \dot{I}^1 &= F_0[I^0,\phi_1^0+\Omega_1(I^0)t,\phi_2^0+\Omega_2(I^0)t], \\ \dot{\phi}_1^1 &= \frac{\partial\Omega_1}{\partial I}(I^0I^1+F_1[I^0,\phi_1^0+\Omega_1(I^0)t,\phi_2^0+\Omega_2 I(I^0)t], \\ \dot{\phi}_2^1 &= \frac{\partial\Omega_2}{\partial I}(I^0)I^1+F_2[I^0,\phi_1^0+\Omega_1(I^0)t,\phi_2^0+\Omega_2(I^0)t]. \end{aligned} \tag{A6}$$

We seek to construct a map that advances the variables $I^{\Delta W},\phi_1^{\Delta W},\phi_2\Delta W$ over a time interval $\tau=1$ from the initial values I^0,ϕ_1^0,ϕ_2^0. The perturbation expansion gives the approximate map

$$\begin{aligned} (I^0,\phi_1^0,\phi_{2^0}\rightarrow[&I^0+\Delta W I^1(\tau),\phi_1^0+\Omega_1(I^0)\tau+\Delta W\phi_1^1(\tau), \\ &\phi_2^0+\Omega_2(I^0)\tau+\Delta W\phi_2^1(\tau)]. \end{aligned} \tag{A7}$$

Expressions for $I^1(\tau),\phi_1^1(\tau)$, and $\phi_2^1(\tau)$ can be obtained by solving Eqs. (A6), which for $\tau=1$ yields

$$\begin{aligned} I^1(1) &= \int_0^1 F_1[I^0,\phi_1^0+\Omega_1 I(^0)t, \\ &\quad \times\phi_2^0+\Omega_2(I^0)t]dt\equiv\widetilde{F}_0(I^0,\phi_1^{0,\phi_2^0}), \\ \phi_1^1(1) &= \int_0^1 F_1[I^0,\phi_1^0+\Omega_1(I^0)t,\phi_2^0+\Omega_2(I^0)t]dt \\ &\quad +\frac{\partial\Omega_1}{\partial I}(I^0)\int_0^1\int_0^t F_0[I^0,\phi_1^0+\Omega_1(I^0)\zeta, \\ &\quad \times\phi_2^0+\Omega_2(I^0)\zeta]d\zeta dt\equiv\widetilde{F}_1(I^0,\phi_1^0,\phi_2^0), \\ \phi_2^1(1) &= \int_0^1 F_2[I^0,\phi_1^0+\Omega_1(I^0)t,\phi_2^0+\Omega_2(I^0)t]dt \\ &\quad +\frac{\partial\Omega_2}{\partial I}I^0\int_0^1\int_0^t F_0[I^0,\phi_1^0+\Omega_1(I^0)\zeta, \\ &\quad \times\phi_2^0+\Omega_2(I^0)\zeta]d\zeta dt\equiv\widetilde{F}_2(I^0,\phi_1^0,\phi_2^0). \end{aligned} \tag{A8}$$

These results yield the final form of the volume-preserving map

$$\begin{aligned} I &\rightarrow I+\Delta W\widetilde{F}_0(I,\phi_1,\phi_2)+O(\Delta W^2), \\ \phi_1 &\rightarrow \phi_1+\Omega_1(I)+\Delta W\widetilde{F}_1(I,\phi_1,\phi_2)+O(\Delta W^2), \\ \phi_2 &\rightarrow \phi_2+\Omega_2(I)+W\widetilde{F}_2(I,\phi_1,\phi_2)+O(\Delta W^2). \end{aligned} \tag{A9}$$

Other, shorter time intervals τ may be used to construct similar maps as required.

[1] H. Stommel, J. Marine Res. **8**, 24 (1949).
[2] M. R. Maxey and S. Corrsin, J. Atmos. Sci. **43**, 1112 (1986).
[3] M. R. Maxey, Phys. Fluids **30**, 1915 (1987).
[4] L. A. Smith and E. A. Spiegel, Lect. Notes Phys. **230**, 306 (1985).
[5] A. Crisanti, M. Falcioni, A. Provenzale, and A. Vulpiani, Phys. Lett. A **150**, 79 (1990).
[6] H. Aref, J. Fluid Mech. **143**, 1 (1984).
[7] V. I. Arnold, C. R. Hebd, Seances Acad. Sci., C **261**, 17 (1965).
[8] T. Dombre, U. Frisch, J. M. Greene, M. Henon, A. Mehr, and A. M. Soward, J. Fluid Mech. **167**, 353 (1986).
[9] L. P. Wang, T. D. Burton, and D. E. Stock, Phys. Fluids A **2**, 1305 (1990).
[10] J. B. McLaughlin, Phys. Fluids A **31**, 2544 (1988).
[11] H. R. Pruppacher and J. D. Klett, *Microphysics of Clouds and Precipitation* (Reidel, Dordrecht, 1978), p. 328.
[12] B. D. Marsh and M. R. Maxey, J. Volcanol. Geotherm. Res. **24**, 95 (1985).
[13] G. B. Jeffery, Proc. R. Soc. London, Ser. A **102**, 161 (1922).
[14] F. P. Bretherton, J. Fluid Mech. **143**, 284 (1962).
[15] J. Happel and H. Brenner, *Low Reynolds Number Hydrodynamics* (Prentice-Hall, Englewood Cliffs, NJ, 1965).
[16] R. H. Davis, Phys. Fluids A **3**, 2051 (1991).
[17] R. Mallier and M. Maxey, Phys. Fluids A **3**, 1481 (1991).
[18] A. J. Szeri, S. Wiggins, and L. G. Leal, J. Fluid Mech. **228**, 207 (1991).
[19] A. J. Szeri, S. Leal, and L. G. Leal, J. Fluid Mech. **242**, 549 (1992).
[20] I. Mezic and S. Wiggins, J. Nonlinear Sci. **4**, 157 (1994).
[21] S. Wiggins, *Introduction to Applied Nonlinear Dynamical Systems and Chaos* (Springer-Verlag, New York, 1990).
[22] C.-Q. Cheng and Y.-S. Sun, Celest. Mech. **47**, 275 (1990).

[23] M. Feingold, L. P. Kadanoff, and O. Piro, J. Stat. Phys. **50**, 529 (1988).
[24] Z. Xia, Ergod. Theoret. Dynam. Syst. **12**, 621 (1992).
[25] M. Henón, Physica D **5**, 412 (1982).
[26] H. Haken, Phys. Lett. **94A**, 71 (1983).
[27] V. J. Oseledec, Trans. Moscow Math. Soc. **19**, 197 (1968).
[28] G. Benettin, L. Galgani, A. Giorgilli, and J. M. Strelcyn, Meccanica **15**, 21 (1980).
[29] J. H. E. Cartwrigh, M. Feingold, and D. Piro, J. Fluid Mech. **316**, 259 (1996).
[30] H. Brenner, J. Colloid Interface Sci. **71**, 189 (1979).
[31] H. Brenner, J. Colloid Interface Sci. **80**, 548 (1981).
[32] L. H. Dill and H. Brenner, J. Colloid Interface Sci. **94**, 430 (1983).
[33] L.-P. Wang, M. R. Maxey, T. D. Burton, and D. E. Stock, Phys. Fluids A **4**, 1789 (1992).